

# The Monoceros radio loop: temperature, brightness, spectral index and distance

V. Borka Jovanović<sup>1\*</sup> and D. Urošević<sup>2\*\*</sup>

<sup>1</sup> Laboratory of Physics (010), Vinča Institute of Nuclear Sciences, P.O. Box 522, 11001 Belgrade, Serbia

<sup>2</sup> Department of Astronomy, Faculty of Mathematics, University of Belgrade, Studentski trg 16, 11000 Belgrade, Serbia

Received 2009 January 12, accepted 2009 April 14

**Key words** surveys – radio continuum: general – ISM: supernova remnants – radiation mechanisms: non-thermal

In this paper we estimated the temperatures and brightnesses of the Monoceros radio loop at 1420, 820 and 408 MHz. Linear spectrum is estimated for mean temperatures versus frequency between 1420, 820 and 408 MHz. The spectral index of Monoceros loop is also obtained. The brightness temperatures and surface brightnesses of the loop are computed using data taken from radio-continuum surveys at the three frequencies. The spectral index of the loop is also obtained from  $T - T$  plots between 1420 - 820, 1420 - 408 and 820 - 408 MHz. The obtained results confirm non-thermal origin of the Monoceros radio loop.

© WILEY-VCH Verlag GmbH & Co. KGaA, Weinheim

## 1 Introduction

The Monoceros filamentary loop nebula was suggested to be a supernova remnant (SNR) by Davies 1963 on the basis of 237 MHz observations. This shell source of radio emission was suspected already by Davies 1963 to be a SNR, while Gebel & Shore 1972 developed this idea into a more detailed study. It was considered as an object similar to major loops when Spoelstra 1973 included it in his study of galactic loops as supernova remnants expanding in the local galactic magnetic field.

Graham et al. 1982 found that the constellation of Monoceros is remarkably rich in extended Galactic radio sources. Large parts of it have been mapped in the radio continuum over a wide range of frequencies. Monoceros Nebula can be found in a catalog of Galactic SNRs listed as G205.5+0.5 (Green 2004, Green 2006). It is S-type remnant (shell remnant), characterized by diffuse, shell-like emission with steep radio spectrum and size of  $\sim 220'$ . Shell type supernova remnants are believed to be particle accelerators to energy up to a few hundred TeV, and it is shown that Monoceros loop is a good candidate for acceleration of particles (Fiasson et al. 2007).

The aim of this paper is to calculate the average brightness temperatures and surface brightnesses of the Monoceros radio loop at 1420, 820 and 408 MHz and to study how these results compare with previous result (Urošević & Milogradov-Turin 1998; Milogradov-Turin & Urošević 1996) and with current theories of supernova remnant evolution. These theories predict that SNRs are at radio frequencies predominantly non-thermal sources which are sp-

reading inside of the hot and low density bubbles made by former supernova explosions or by strong stellar winds (see Salter 1983; McKee & Ostriker 1977 and references therein).

Spectrum (temperature versus frequency) have been plotted and this result is used to determine spectral index of the Monoceros loop.

## 2 Analysis

### 2.1 Data

In this paper we used observations from several radio-continuum surveys given in "Flexible Image Transport System" (*FITS*) format which are available on MPIfR's Survey Sampler ("Max-Planck-Institut für Radioastronomie", Bonn). This is an online service (<http://www.mpifr-bonn.mpg.de/survey.html>), which allows users to pick a region of the sky and obtain images and observed data (in *FITS* format) at a number of wavelengths. User can choose a coordinate system, projection type and a survey. The radio continuum surveys at 1420, 820 and 408 MHz provided the database for computing brightness temperatures ( $T_b$ ). The 1420-MHz Stockert survey (Reich & Reich 1986) has the angular resolution of  $35'$ , the 820-MHz Dwingeloo survey (Berkhuijsen 1972)  $1^\circ.2$  and the 408-MHz all-sky survey (Haslam et al. 1982)  $0^\circ.85$ . The corresponding observations are given at the following rates for both  $l$  and  $b$ :  $\frac{1^\circ}{4}$  at 1420 MHz,  $\frac{1^\circ}{2}$  at 820 MHz and  $\frac{1^\circ}{3}$  at 408 MHz. The effective sensitivities are about 50 mK  $T_b$ , 0.20 K and about 1.0 K, respectively.

\* Corresponding author: e-mail: vborka@vinca.rs

\*\* e-mail: dejanu@matf.bg.ac.yu

## 2.2 Method

We extracted observed brightness temperatures from *FITS* format into ASCII data files and after that, these data files have been processed by our software, i.e. we have developed several programs in C and FORTRAN in order to obtain results presented in this paper.

The area of Monoceros loop is very difficult to determine precisely due to great influence of background radiation and superposed external sources, such as Rosette Nebula (Graham et al. 1982; Aharonian et al. 2004, Aharonian et al. 2007; Kim et al. 2007). Therefore, some authors made very rough estimates for the shape of this loop, representing it by fitted circles (see e.g. Aharonian et al. 2004; Kim et al. 2007). In order to make better estimates for the loop boundaries, we analyzed temperature profiles (see Figure 1) for different values of Galactic latitude ( $b$ ) between  $-6^\circ$  and  $6^\circ$ , and for Galactic longitude ( $l$ ) from  $212^\circ$  to  $198^\circ$ . As one can see in Figure 1, there are two temperature peaks. The lower one corresponds to the total brightness temperature of the loop (including background radiation), while the higher one corresponds to superposed external sources. We denoted the minimum and maximum brightness temperature of the lower peak by  $T_{\min}$  and  $T_{\max}$ , respectively. These temperature limits enable us to distinguish the loop from background and also from external sources, and their values are given in Table 1. Moreover, using the temperature profiles we found that the Monoceros loop is located in this sky region:  $l \in [210^\circ, 200^\circ]$  and  $b \in [-6^\circ, 5^\circ]$ .

The area of Monoceros loop is enclosed with brightness temperature contours (see Figure 2). These contour lines correspond to the minimum and maximum brightness temperatures which define its borders (see Table 1), and 9 contours in between. We have subtracted the background radiation, as well as the superposed radiation, in order to derive the mean brightness temperature of the SNR alone (see Borka 2007 and Borka, Milogradov-Turin & Urošević 2008).

For deriving temperatures over the Monoceros loop, the areas used for the individual spurs were obtained from the radio continuum maps at three frequencies: 1420 MHz (Reich & Reich 1986), 820 MHz (Berkhuijsen 1972) and 408 MHz (Haslam et al. 1982). The areas over which an average brightness temperature is determined at each of the three frequencies are taken to be as similar as possible within the limits of measurement accuracy. Temperature limits  $T_{\min}$  and  $T_{\max}$ , given in Table 1, are the lower and the upper temperature values:  $T_{\min}$  is the lower temperature limit between the background and the spur, while  $T_{\max}$  is the upper temperature limit between the spur and superposed confusing sources. In this manner, background radiation was considered as radiation that would exist if there were no spurs. If the value of  $T_{\min}$  ( $T_{\max}$ ) is changed by some small value (approximately 0.1 K for 1420 MHz and more for other frequencies), the brightness contours become significantly different. For evaluating brightness temperature of the background, we used all measured values below  $T_{\min}$ , inside the

corresponding intervals of  $l$  and  $b$ , and lying on the outer side of a loop. The value of  $T_b$  is approximately constant near a loop. For evaluating the brightness temperature of a loop including the background, we used all measured values between  $T_{\min}$  and  $T_{\max}$  inside the corresponding regions of  $l$  and  $b$ . Mean brightness temperature for loop is found by subtracting the mean value of background brightness temperature from the mean value of the brightness temperature over the area of the loop. After deriving the temperature, we derived the surface brightness by:

$$\Sigma = (2k\nu^2/c^2)T_b \quad (1)$$

where  $k$  is Boltzmann constant and  $c$  is the speed of light. Results are given in Table 1.

The surface brightnesses of SNRs must be above the sensitivity limit of the observations and must be clearly distinguishable from the Galactic background emission (Green 1991). Therefore, the data from the fainter parts of the loops (which are very low surface brightness SNRs) are not taken into account because it is very difficult to resolve them from the background. On the other hand, this would significantly reduce brightness of entire loop and there is a general trend that fainter SNRs tend to be larger (Green 2005). For evaluation brightness temperatures over the spurs we had to take into account background radiation (Webster 1974). Borders enclosing the spurs are defined to separate the spur and its background.

The measured data have different resolutions for different frequencies (see §2.1), and therefore in order to obtain  $T - T$  plots the data are retabulated so the higher resolution maps are convolved to the resolution of the lowest resolution map. In that way we convolved data at 1420 and 408 MHz to  $0.5 \times 0.5$  resolution, which is the sampling rate of the 820 MHz survey. These retabulated data are presented in Figure 4 for the following frequencies: 1420 MHz (top left), 820 MHz (top right), 408 MHz (bottom left). Then, for each frequency pair we used only the common points (with the same  $(l, b)$ ) which belong to the loop area at both frequencies (see Figure 4, bottom right). In that way we reduced loop area to the same area for different frequencies. The obtained  $T - T$  plots for three pairs of frequencies (between 1420-820, 1420-408 and 820-408 MHz) enabled calculating the spectral indices. For each of the three frequency pairs, by interchanging the dependent and independent variables we have obtained two  $\beta$  values for each pair and the mean value of these fit results is adopted as the radio spectral index, as suggested in Uyaniker et al. 2004.

## 3 Results and discussion

The average brightness temperatures and surface brightnesses of Monoceros radio loop at the three frequencies are given in Table 1.

Spectrum shows how temperature depends on the frequency:

$$\log T = \log K - \beta \log \nu \quad (2)$$

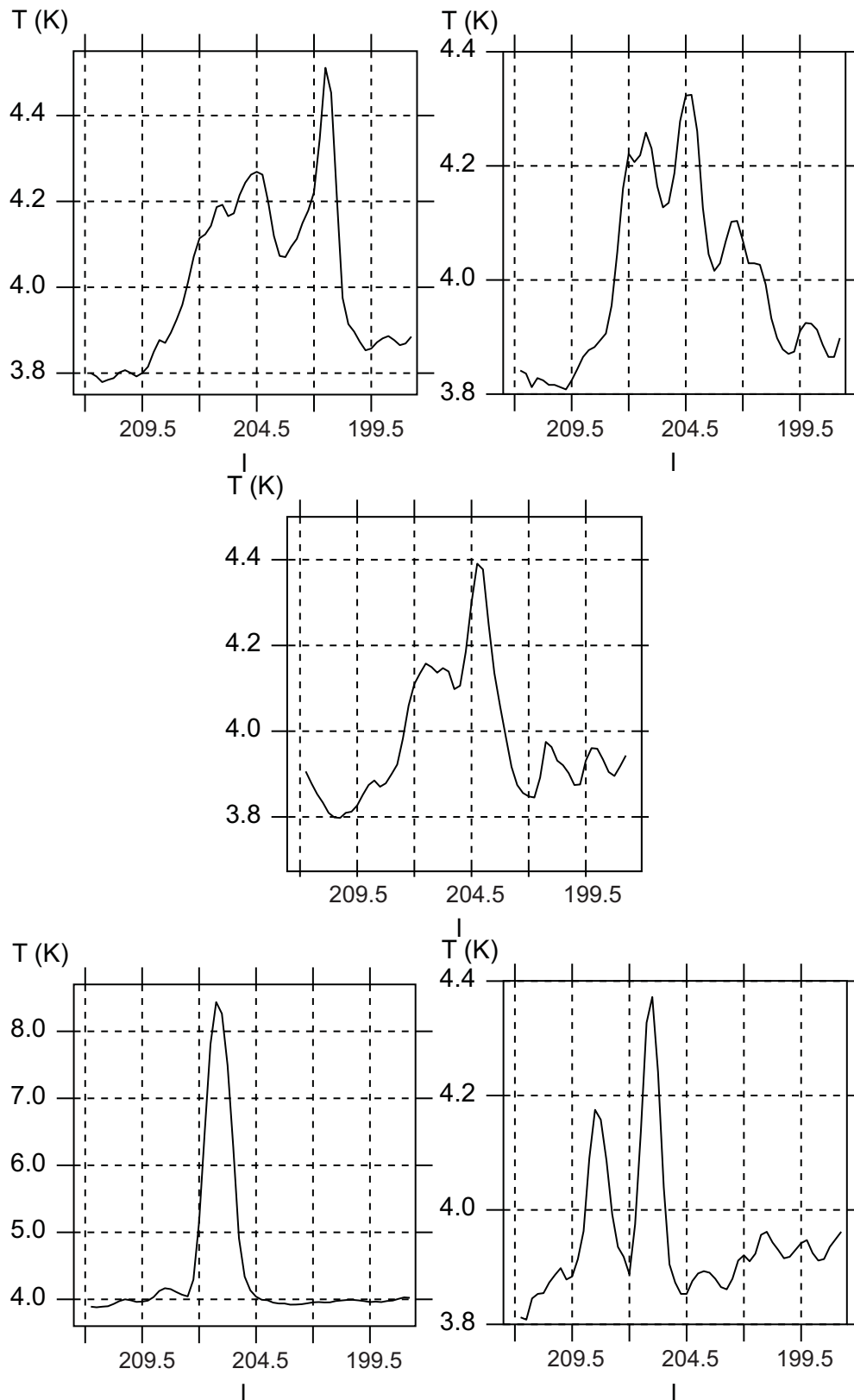


**Fig. 1** Temperature profiles at 1420 MHz for Galactic longitude from  $212^\circ$  to  $198^\circ$  and for the following values of Galactic latitude:  $1.5^\circ$  (top left),  $1^\circ$  (top right),  $0^\circ$  (middle),  $-2^\circ$  (bottom left) and  $-3^\circ$  (bottom right). Temperatures are given in K, and Galactic longitudes in degrees.

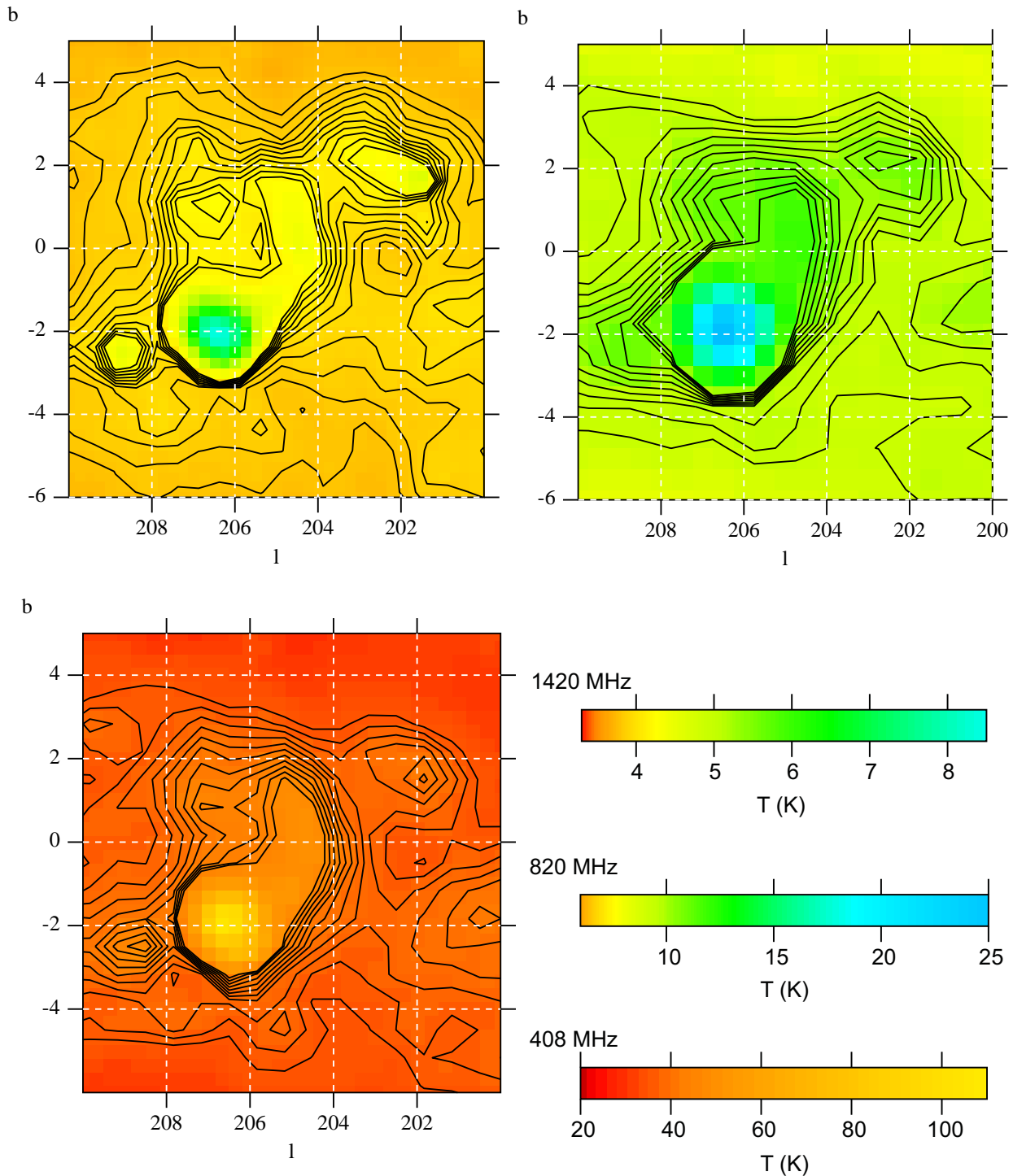


**Fig. 2** The map of a region in Monoceros, in new galactic coordinates ( $l$ ,  $b$ ). Contours of the brightness temperatures  $T_b$  are plotted. **Top left:** the 1420 MHz map with contours of  $T_b$  given in units of K. The contours are plotted every 0.04 K starting from the lowest temperature of 3.8 K up to 4.2 K. **Top right:** the 820 MHz map with  $T_b$  in K. The contours are plotted every 0.19 K starting from 8.8 K up to 10.7 K. **Bottom left:** the 408 MHz map with  $T_b$  in K. The contours are plotted every 1.1 K starting from 36 K up to 47 K. **Bottom right:** temperature colorbars for 1420, 820 and 408 MHz, all in K.

**Table 1** Temperatures and brightnesses of Monoceros radio loop at 1420, 820 and 408 MHz.

| Frequency<br>(MHz) | Temperature limits<br>$T_{\min}, T_{\max}$ (K) | Temperature<br>(K) | Brightness<br>( $10^{-22}$ W/(m <sup>2</sup> Hz Sr)) |
|--------------------|--|--------------------|--|
| 1420               | 3.8, 4.2                                       | $0.18 \pm 0.05$    | $1.09 \pm 0.30$                                      |
| 820                | 8.8, 10.7                                      | $0.90 \pm 0.20$    | $1.85 \pm 0.40$                                      |
| 408                | 36, 47   | $5.2 \pm 1.0$      | $2.63 \pm 0.50$                                      |

where  $K$  is a constant, and  $\beta$  is radio spectral index.

The spectrum was generated using mean temperatures at three different frequencies. This best-fit straight line spectrum enables calculation of spectral index as negative value of the line's direction coefficient. The spectrum is shown in Figure 3. Relative errors of the measurements  $\Delta \log T = \frac{\Delta T}{T \ln 10}$  are presented by error bars, where  $\Delta T$  are the corresponding absolute errors given in Table 1. Obtained value  $\beta = 2.70 \pm 0.14$  (greater than 2.2) confirm non-thermal origin of Monoceros loop emission. The value for the brightness temperature spectral index of the Monoceros loop is rather steep (about 2.7). This is at the high end of the spectral index distribution for SNRs as suggested in Clark & Caswell 1976.

From the relation ( $T - T$  plot):

$$T_{\nu 1}/T_{\nu 2} = (\nu_1/\nu_2)^{-\beta} \quad (3)$$

$\beta$  can be determined as

$$\beta = \log(a_{12})/\log(\nu_1/\nu_2), \quad (4)$$

where  $a_{12}$  is direction coefficient of line  $T_{\nu 2}(T_{\nu 1})$ .

Because of the influence of superposed sources to the loop and because it is hard to estimate precise loop's borders, we present how spectral indices vary for different  $b$ . Variations of spectral indices between the three frequency pairs obtained from T-T plots, distributed over Galactic latitudes, are given in Tables 2-4. For some Galactic latitudes, there is a large dispersion of the points in  $T - T$  graphs so they are not suitable for calculation of spectral index; we did not calculate  $\beta$  for them and it is denoted with "-". The averaged values of radio spectral indices are given in Table 5. Examples of  $T - T$  plots between 1420-820, 1420-408 and 820-408 MHz for longitude  $b = 1^\circ$  are given in Figure 5. The average value of spectral index from  $T - T$  is  $\langle \beta_{TT} \rangle = 2.63 \pm 0.30$ . It can be noticed that this value agrees well with the corresponding value obtained from spectrum, as expected (see Uyaniker et al. 2004). Then we calculated mean value of spectral index between 1420, 820 and 408 MHz (regarding spectrum and  $T - T$  graphs)  $\langle \beta \rangle = 2.66 \pm 0.20$ . With this  $\langle \beta \rangle$  we reduced  $\Sigma_\nu$  to 1000 MHz (Table 6) according to relation:

$$\Sigma_{1\text{GHz}}/\Sigma_{\nu\text{GHz}} = (\nu/1)^{(\beta-2)}. \quad (5)$$

In Graham et al. 1982, the value  $\beta = 2.47 \pm 0.06$  of radio spectral index of this loop was derived from the radio continuum spectrum between two frequencies: 111 and 2700 MHz, and we calculated spectrum at three frequencies and also derived  $T - T$  graphs which represent different method.

**Table 2** Variations of spectral indices between 1420 and 820 MHz obtained from T-T plots, distributed over Galactic latitudes.

| latitude ( $^\circ$ ) | $\beta(1420 - 820)$ | $\beta(820 - 1420)$ |
|-----------------------|---------------------|---------------------|
| -5.0                  | -                   | -                   |
| -4.5                  | -                   | -                   |
| -4.0                  | -                   | -                   |
| -3.5                  | -                   | -                   |
| -3.0                  | $1.92 \pm 0.82$     | $4.54 \pm 0.82$     |
| -2.5                  | $3.86 \pm 0.46$     | $4.84 \pm 0.46$     |
| -2.0                  | $3.47 \pm 0.31$     | $4.07 \pm 0.31$     |
| -1.5                  | $2.96 \pm 0.73$     | $5.02 \pm 0.73$     |
| -1.0                  | $1.96 \pm 0.55$     | $3.31 \pm 0.55$     |
| -0.5                  | $2.61 \pm 0.39$     | $3.36 \pm 0.39$     |
| 0                     | $2.39 \pm 0.22$     | $2.73 \pm 0.22$     |
| 0.5                   | $2.49 \pm 0.28$     | $3.09 \pm 0.28$     |
| 1.0                   | $2.42 \pm 0.26$     | $2.85 \pm 0.26$     |
| 1.5                   | $2.74 \pm 0.27$     | $3.13 \pm 0.27$     |
| 2.0                   | $2.62 \pm 0.26$     | $3.02 \pm 0.26$     |
| 2.5                   | $1.59 \pm 0.41$     | $2.69 \pm 0.41$     |
| 3.0                   | $1.26 \pm 0.43$     | $2.41 \pm 0.43$     |

Distances to the SNRs can be inferred from positional coincidences with HI, HII regions and molecular clouds, OB associations, or pulsars or from measuring optical velocities and proper motions. Where there is no direct distance determination, estimates can be made for shell remnants by utilizing the radio surface brightness-to-diameter relationship ( $\Sigma - D$ ) (Case & Bhattacharya 1998 and references therein). The mean surface brightness at a specific radio frequency,  $\Sigma_\nu$  is a distance-independent parameter and, to a first approximation, is an intrinsic property of the SNR (Shklovskii 1960).

Using a set of 172 SNRs as calibrators, for which reliable distance values were determined, Urošević 2002 has constructed the following relation between the surface brightness ( $\Sigma$ ) and diameter ( $D$ ):

$$\Sigma_{1\text{GHz}} = 2.76 \times 10^{-16} D^{-3.02} \quad (6)$$

This relation, combining the Galactic and extragalactic SNRs (master relation), also includes four main Galactic radio loops (Loops I - IV).

It is shown (Odegard 1986) that there is diffuse emission with the filaments located in the western half of Monoceros loop (overlapping with Rosette Nebula) and in the eastern part (dust cloud L1631). There is also a peak in the 2700 MHz emission in the eastern edge for which Graham et al. 1982 suggested to be a HII region. In Aharonian et al. 2007

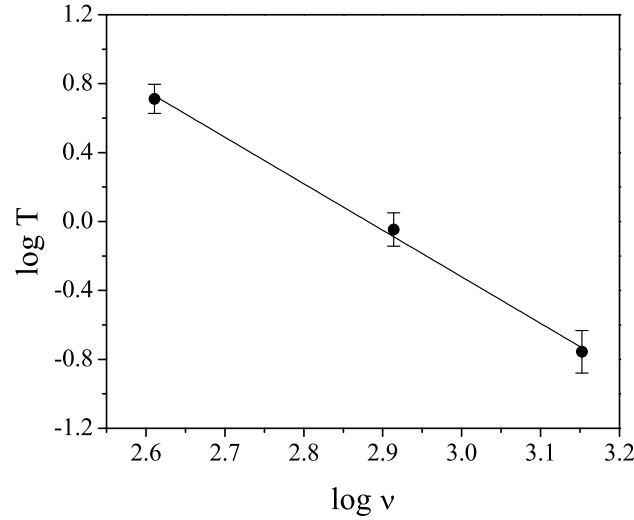


**Fig. 3** Monoceros loop spectrum: temperature versus frequency, for three measurements – at 408, 820 and 1420 MHz.

**Table 3** Variations of spectral indices between 1420 and 408 MHz obtained from T-T plots, distributed over Galactic latitudes.

| latitude (°) | $\beta(1420 - 408)$ | $\beta(408 - 1420)$ |
|--------------|---------------------|---------------------|
| -5.0         | $1.92 \pm 0.24$     | $2.32 \pm 0.24$     |
| -4.5         | $2.14 \pm 0.33$     | $3.15 \pm 0.33$     |
| -4.0         | $2.35 \pm 0.12$     | $2.62 \pm 0.12$     |
| -3.5         | -                   | -                   |
| -3.0         | $2.48 \pm 0.19$     | $3.03 \pm 0.19$     |
| -2.5         | $2.91 \pm 0.13$     | $3.14 \pm 0.13$     |
| -2.0         | $2.58 \pm 0.11$     | $2.78 \pm 0.11$     |
| -1.5         | $2.55 \pm 0.14$     | $2.82 \pm 0.14$     |
| -1.0         | $2.55 \pm 0.08$     | $2.65 \pm 0.08$     |
| -0.5         | $2.69 \pm 0.07$     | $2.76 \pm 0.07$     |
| 0            | $2.58 \pm 0.10$     | $2.75 \pm 0.10$     |
| 0.5          | $2.39 \pm 0.16$     | $2.78 \pm 0.16$     |
| 1.0          | $2.40 \pm 0.19$     | $2.82 \pm 0.19$     |
| 1.5          | $2.16 \pm 0.22$     | $2.65 \pm 0.22$     |
| 2.0          | $2.19 \pm 0.25$     | $2.80 \pm 0.25$     |
| 2.5          | -                   | $3.23 \pm 0.89$     |
| 3.0          | -                   | -                   |

**Table 4** Variations of spectral indices between 820 and 408 MHz obtained from T-T plots, distributed over Galactic latitudes.

| latitude (°) | $\beta(820 - 408)$ | $\beta(408 - 820)$ |
|--------------|--------------------|--------------------|
| -5.0         | $2.38 \pm 0.51$    | $3.29 \pm 0.51$    |
| -4.5         | $1.39 \pm 0.89$    | $4.20 \pm 0.89$    |
| -4.0         | $1.71 \pm 0.49$    | $3.22 \pm 0.49$    |
| -3.5         | $1.12 \pm 0.56$    | $2.74 \pm 0.56$    |
| -3.0         | $1.87 \pm 0.33$    | $2.74 \pm 0.33$    |
| -2.5         | $1.57 \pm 0.28$    | $2.07 \pm 0.28$    |
| -2.0         | $1.47 \pm 0.25$    | $1.95 \pm 0.25$    |
| -1.5         | $1.24 \pm 0.35$    | $2.07 \pm 0.35$    |
| -1.0         | $2.23 \pm 0.31$    | $2.87 \pm 0.31$    |
| -0.5         | $2.44 \pm 0.17$    | $2.67 \pm 0.17$    |
| 0            | $2.49 \pm 0.10$    | $2.58 \pm 0.10$    |
| 0.5          | $2.23 \pm 0.12$    | $2.36 \pm 0.12$    |
| 1.0          | $2.22 \pm 0.18$    | $2.50 \pm 0.18$    |
| 1.5          | $1.91 \pm 0.25$    | $2.36 \pm 0.25$    |
| 2.0          | $1.96 \pm 0.18$    | $2.29 \pm 0.18$    |
| 2.5          | -                  | $3.21 \pm 0.72$    |
| 3.0          | -                  | -                  |

it is said that the complex Monoceros loop/Rosette Nebula region contains several potential sources of very-high-energy  $\gamma$  ray emission and that the interaction of the SNR with a compact molecular cloud is possible. Because of possible influence with molecular clouds and HII region, we also take  $\Sigma - D$  relation from Arbutina et al. 2004 adjusted for molecular clouds:

$$\Sigma_{1\text{GHz}} = 1.1 \times 10^{-15} D^{-3.5} \quad (7)$$

They have taken 14 shell-type Galactic SNRs associated with large molecular clouds.

Using the relations derived by Urošević 2002 and Arbutina et al. 2004, we computed diameter of the loop and then we computed distance as:

$$r = D / (2 \sin \Theta), \quad (8)$$

**Table 5** The average radio spectral indices between 1420, 820 and 408 MHz obtained from T-T plots.

| Frequency pair (MHz) | $\beta_{TT}$    |
|----------------------|-----------------|
| 1420 - 820           | $2.98 \pm 0.40$ |
| 1420 - 408           | $2.62 \pm 0.20$ |
| 820 - 408            | $2.29 \pm 0.34$ |

**Table 6** Brightnesses of Monoceros radio loop reduced to 1000 MHz using  $\beta = 2.66 \pm 0.20$ .

| Frequency (MHz) | Brightness at 1000 MHz ( $10^{-22} \text{ W}/(\text{m}^2 \text{ Hz Sr})$ ) |
|-----------------|--|
| 1420            | $1.37 \pm 0.50$  |
| 820             | $1.63 \pm 0.30$  |
| 408             | $1.45 \pm 0.03$  |

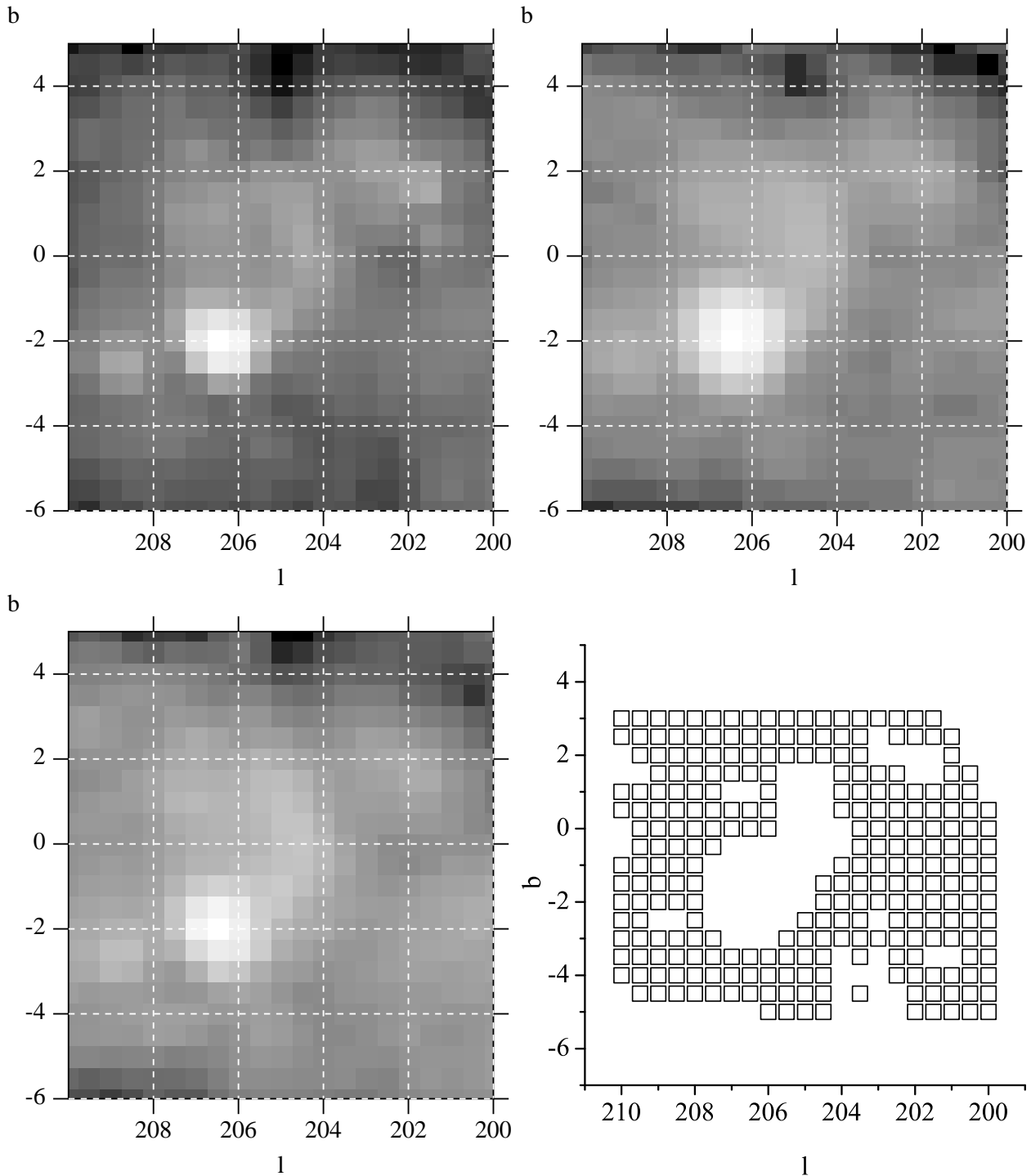


**Fig. 4** The data retabulated to  $0^\circ.5 \times 0^\circ.5$  resolution, for the following frequencies: 1420 MHz (**top left**), 820 MHz (**top right**) and 408 MHz (**bottom left**). **Bottom right**: the common pixels which belong to the loop area at all frequencies.

with angular radius ( $\Theta$ ) taken from Urošević & Milogradov-Turin 1998. The results are given in Table 7.

It can be noticed that there is the influence of molecular cloud on Monoceros loop (Graham et al. 1982, Aharonian et al. 2007). If that influence constantly existed during the loop's evolution, then for distance calculation it is more suit-

able  $\Sigma - D$  relation by Arbutina et al. 2004. If not, then it is more suitable to use relation by Urošević 2002.

For the distance to this loop, mean optical velocity suggests 0.8 kpc, and low frequency radio absorption suggests 1.6 kpc (Graham et al. 1982, Odegard 1986, Green 2006). With our calculated radio spectral index  $\beta = 2.66 \pm 0.20$ ,

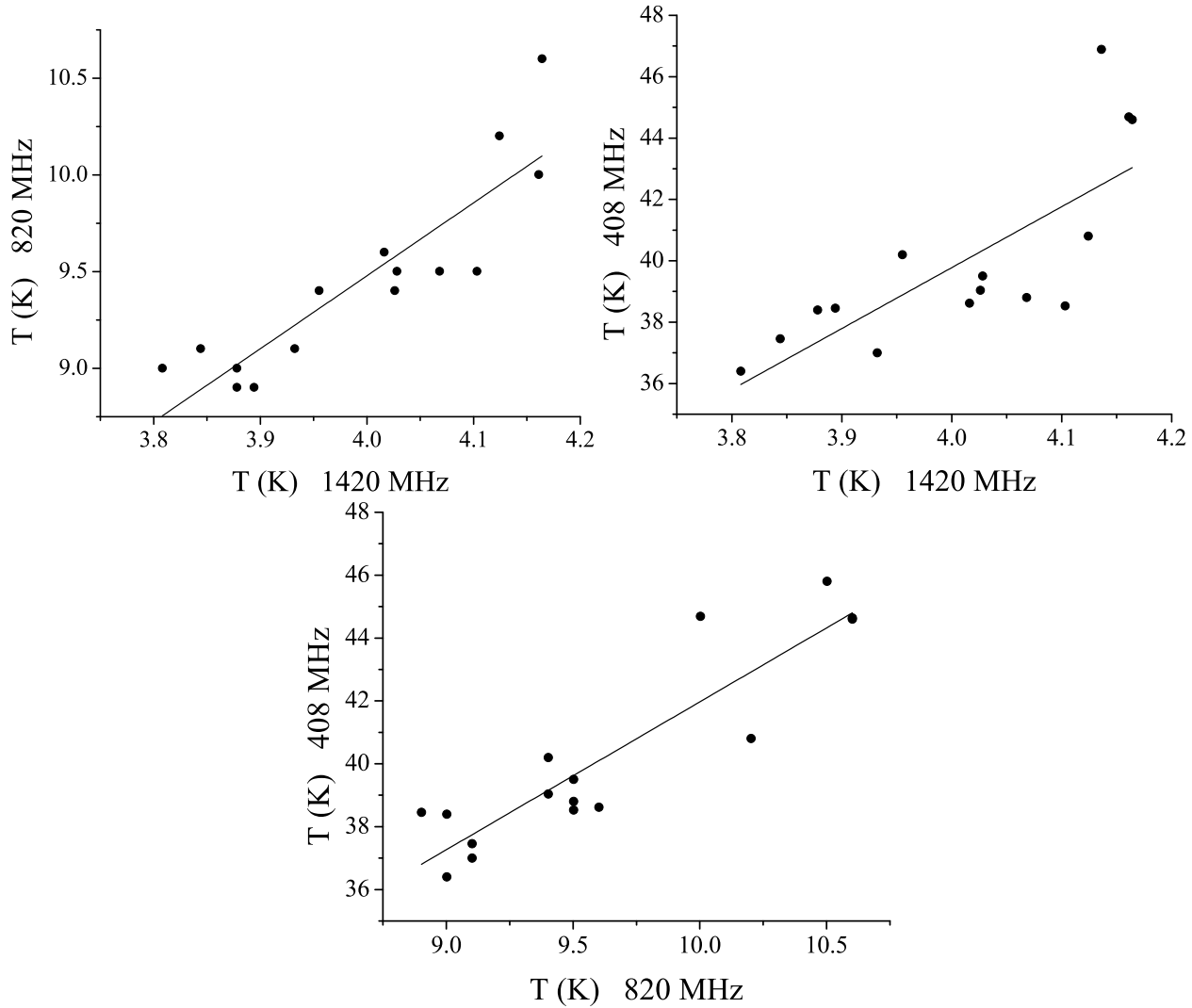


**Fig. 5** **Top left:** T-T plot between 1420 and 820 MHz for Monoceros loop at latitude  $b = 1^\circ$ , in longitude range  $[210^\circ, 200^\circ]$ . **Top right:** the same as top left, but between 1420 and 408 MHz. **Bottom:** the same as top left, but between 820 and 408 MHz.

**Table 7** Diameters  $D$  (pc) and distances  $r$  (pc) of Monoceros radio loop derived from the  $\Sigma - D$  relation given by Urošević 2002 and by Arbutina et al. 2004.

| Relation | $D$ (pc)     | $r$ (pc)       |
|----------|--------------|----------------|
| (6)      | $119 \pm 18$ | $1630 \pm 250$ |
| (7)      | $92 \pm 14$  | $1250 \pm 190$ |

we calculated distance to this loop using our derived brightnesses. The results are given in Table 7.

## 4 Conclusions

In this paper we calculated the brightness temperatures and surface brightnesses of the Monoceros radio loop at 1420, 820 and 408 MHz. Linear spectrum is estimated for mean temperatures versus frequency between 1420, 820 and 408 MHz. It is the first time that the brightness temperatures of

Monoceros loop are calculated at 820 and 408 MHz frequencies from the observational data. We sampled much more points (more than 1 000) at 1420 MHz than in previous papers (95 points) (Urošević & Milogradov-Turin 1998, Milogradov-Turin & Urošević 1996). Also, the brightness temperature is now derived using the different method. The temperature of this radio loop at 1420 MHz is in good agreement with the result obtained in Urošević & Milogradov-Turin 1998.

We present the radio continuum spectrum of the Monoceros loop using average brightness temperatures at three different frequencies. As it can be seen from Figure 3, given linear fit provides reliable spectral index. Also, we present the  $T - T$  plots which enables also calculation of spectral index.

The effective sensitivity of the brightness temperatures are: 50 mK for 1420 MHz, 0.2 K for 820 MHz, and about 1.0 K for 408 MHz. The most precise measurements (the



least relative errors) are in case of 1420 MHz, so positions of the brightness temperature contours of the loop are the most realistic for this frequency. The brightnesses of Monoceros loop at 1420 and 820 and 408 MHz are in good agreement when reduced to 1 GHz.

With our derived brightnesses, we calculated new diameters and distances to this loop at the three frequencies: 1420, 820 and 408 MHz and then estimated some average distance. We used empirical  $\Sigma - D$  relations for supernova remnants by Urošević 2002 and Arbutina et al. 2004. The estimated distance of the Monoceros radio loop is in good agreement with the earlier results (Guseinov et al. 2004; Green 2006: 1.6 kpc).

The spectral index analysis confirms non-thermal origin of Monoceros radio loop.

*Acknowledgements.* This research is part of the projects: "Gaseous and stellar component of galaxies: interaction and evolution" (No. 146012) and "Physics and chemistry with ion beams" (No. 451-01-00049) supported by the Ministry of Science of Republic of Serbia.

## References

- Aharonian, F. A., et al. (HEGRA collaboration) : 2004, A&A 417, 973
- Aharonian, F. A., et al. (HESS collaboration): 2007, A&A 469, L1
- Arbutina, B., Urošević, D., Stanković, M., Tešić, Lj.:2004, MNRAS 350, 346
- Berkhuijsen, E. M.: 1972, A&AS 5, 263
- Borka, V.: 2007, MNRAS 376, 634
- Borka, V., Milogradov-Turin, J., Urošević, D.: 2008, AN 329, 397
- Case, G. L., Bhattacharya, D.: 1998, ApJ 504, 761
- Clark, D. H., Caswell, J. L.: 1976, MNRAS 174, 267
- Davies, R. D.: 1963, Observatory 83, 172
- Fiasson, A., Hinton, J. A., Gallant, Y., Marcowith, A., Reimer, O., Rowell, G. (for the H.E.S.S. Collaboration): 2007, arXiv: astro-ph/0709.2550
- Gebel, W. L., Shore, S. N.: 1972, ApJ 172, L9
- Graham, D. A., Haslam, C. G. T., Salter, C. J., Wilson, W. E.: 1982, A&A 109, 145
- Green, D. A.: 1991, PASP 103, 209
- Green, D. A.: 2004, BASI 32, 335
- Green, D. A.: 2005, MemSAI 76, 534
- Green, D. A.: 2006, A Catalogue of Galactic Supernova Remnants (2006 April version), Cavendish Laboratory, Cambridge, UK.
- Guseinov, O. H., Ankay, A., Tagieva, S. O.: 2004, Serb. Astron. J. 168, 55
- Haslam, C. G. T., Salter, C. J., Stoffel, H., Wilson, W. E.: 1982, A&AS 47, 1
- Kim I.-J., Min, K.-W., Seon, K.-I., Park, J.-W., Han, W., Park, J.-H., Nam, U.-W., Edelstein, J., Sankrit, R., Korpela, E. J.: 2007, ApJ 665, L139
- McKee, C. F., Ostriker, J. P.: 1977, ApJ 218, 148
- Milogradov-Turin, J., Urošević, D.: 1996, Publ. Astron. Obs. Belgrade 54, 47
- Odegard, N. 1986, ApJ 301, 813
- Reich, P., Reich, W.: 1986, A&AS 63, 205
- Salter, C. J.: 1983, BASI 11, 1
- Shklovskii, I. S.: 1960, Soviet Astronomy - AJ 4, 243
- Spoelstra, T. A. Th. : 1973, A&A 24, 149
- Urošević, D.: 2002, Serb. Astron. J. 165, 27
- Urošević, D., Milogradov-Turin, J.: 1998, Serb. Astron. J. 157, 35
- Uyaniker, B., Reich, W., Yar, A., Furst, E.: 2004, A&A 426, 909
- Webster, A. S.: 1974, MNRAS 166, 355